Aero-Optical Environment Around a Cylindrical Turret with a Flat Window

Stanislav Gordeyev,* Jacob A. Cress,† and Eric J. Jumper‡
University of Notre Dame, Notre Dame, Indiana 46556
and
Alan B. Cain§
Innovative Technology Applications Company, LLC, Chesterfield, Missouri 63006-6971

Optical aberrations over a cylindrical turret with a flat window were measured using a two-dimensional wavefront sensor and a Malley probe, as a function of laser beam elevation angle. Topology of the flow around the cylinder was extensively studied using hot wires. It was found that, depending on the window elevation angle, the flow either had a weak separation bubble followed by a reattached boundary layer or a strong separation with a large recirculation region behind the cylindrical turret. Optical aberrations were shown to be consistent with flow topology. It was found that optical aberrations were high around an elevation angle of 100 deg and at large lookback elevation angles.

Nomenclature

Ap	=	laser beam aperture
Corr	=	velocity–optical path difference correlation function
D	=	cylinder diameter
f	=	frequency
K_{GD}	=	Gladstone–Dale constant
L	=	separation bubble size
M	=	Mach number
M_{free}	=	incoming Mach number
M_{turret}	=	Mach number over the cylindrical turret
n, n'	=	index of refraction and its fluctuating component
OPD_{rms}	=	spatial root-mean square of optical path difference
R	=	cylinder radius
s	=	integration variable
t	=	time
U	=	time-averaged streamwise velocity component
U_{free}, U_∞	=	freestream speed
u_{rms}	=	root-mean-squared streamwise velocity component
u_{rms}^{max}	=	maximum value of u_{rms} at a given streamwise location
x, y	=	turret's coordinate system
δ	=	incoming boundary-layer displacement thickness
η	=	distance in normal direction from flat window
Θ	=	incoming boundary-layer momentum thickness
θ	=	azimuthal angle
ρ	=	freestream density
ρ_{SL}	=	sea level density, $1.225 \text{ kg} \cdot \text{m}^{-3}$
ρ'	=	density fluctuations

*Associate Research Professor, Department of Aerospace and Mechanical Engineering. Senior Member AIAA.
†Graduate Research Assistant, Department of Aerospace and Mechanical Engineering. Student Member AIAA.
‡Professor, Department of Aerospace and Mechanical Engineering. Fellow AIAA.
§President. Associate Fellow AIAA.

I. Introduction

TURBULENT flows generate nonuniform and highly unsteady density fields. Changes in the density field directly effect the index-of-refraction field:

$$n'(\boldsymbol{x}, t) = K_{GD}\rho'(\boldsymbol{x}, t) \tag{1}$$

where n' and ρ' are the fluctuations in index of refraction and density, respectively, and K_{GD} is the Gladstone–Dale constant. If a collimated laser beam is propagated through this variable index-of-refraction field, different regions of the beam are advanced while other regions are retarded, resulting in an aberrated beam. The disruption of laser energy from the ideal diffraction-limited pattern can greatly reduce the usefulness of the laser system. When the laser is carried aboard an aircraft, there are two main causes of beam aberration: the turbulent airflow immediately around the aircraft (layer thickness on the same order of or less than the beam aperture), coined the aero-optic problem by Gilbert and Otten [1], and the many orders of magnitude longer atmospheric-propagation problem from the aircraft to the target. Modern beam control and adaptive optics can compensate for much of the low-frequency effects of the atmospheric problem; for aero-optic-induced beam degradation, however, the aberrations of the turbulent flow occur at frequencies on the order of kilohertz, placing beam control outside of current correction capabilities. The relatively high frequencies of adaptive optic systems can be reduced if the near-field flow is properly conditioned or regularized [2].

Hemispherical turrets are of particular interest due to their presumed large field of regard. On the other hand, a complex flow topology around turrets and the associated aero-optical effects not only render the aft field of regard unusable but present a difficult problem to study [3]. For a turret with a conformal window, aero-optical aberrations are consistently lower than for a turret with a flat window. Also, in the case when the turret has a flat aperture window, the flow is also viewing-angle dependent.

In [4], the optically aberrating environment around a generic hemisphere-on-cylinder turret with a flat window was experimentally studied at limited elevation and azimuthal angles at several subsonic Mach numbers. It was found that the flow topology, and hence the physical mechanism, of optical distortions strongly depends on the angle between the window plane and the incoming flow. When the flow over the flat window faces a moderate or strong adverse pressure gradient, it separates. At the lowest azimuthal and elevation angles, the adverse pressure gradient is localized to the geometric discontinuity at the upstream edge of the window, and the separated flow results in an unsteady separation bubble and subsequent reattached flow over the window. In this case, the aberrating character of the flow is physically similar to that of shallow

ramps tested in [5]. When the angle is sufficiently strong to fully separate the flow, the aberrating character of the resulted separated shear layer is close to that of any experimentally studied canonical separated shear layers [6].

To better understand the underlying physics of optical aberrations in the separated region over the windows of flat-windowed turrets, it is important to note that one of the dominant mechanisms of creating aero-optical distortions is flow separation caused by the slope discontinuity between the turret body and the flat window. To study this effect, a simpler experiment with a flat-windowed cylindrical turret was conducted, since many of the same flow characteristics are present in this configuration, as on the more complicated flat-window hemispherical turret [7]. Results from the flat-window cylindrical turret are presented here. The experimental setup is given in Sec. II. Extensive velocity measurements around the cylindrical turret at different elevation angles, combined with optical measurements using a Shack–Hartmann wavefront sensor, were conducted, and the results are presented and discussed in Sec. III. Also, to further understand the unsteady nature of aero-optical effects caused by the cylindrical turret with the flat window, correlations between the local velocity and aero-optical distortions taken by the Malley probe were conducted, and these results are also discussed in Sec. III. Also, results were compared with results from the flat-window hemispherical turret, and they were shown to be qualitatively similar to the flow structure over the flat window on the simplified cylindrical turret.

II.   Experimental Setup

All tests were performed in transonic facilities at Hessert Laboratory for Aerospace Research, University of Notre Dame. The facilities were described in detail in Gordeyev at al. [8], and an interested reader is referred to this reference for a complete discussion. Except for portions requiring high-quality optical windows, the rotating cylindrical-turret test section was made of clear Plexiglas. A general view and detailed dimensions of the test section with the flat-window cylindrical turret are shown in Fig. 1; not shown in the upper portion of the test section is the optical window used for making Shack–Hartmann sensor wavefront measurements. The test section was 4 in. wide, and it is 4 in. tall upstream of the cylinder and opens up to a taller 5.625-in.-high test section downstream of the cylindrical turret. This test section geometry was chosen to minimize the blockage effect of the cylinder on the incoming flow yet have a realistic cylinder–wall junction downstream of the turret. The 4-in.-diam by 4-in.-span cylinder was able to be freely rotated to elevation angles between 90 and 180 deg. The elevation angle is defined as the angle between the outward normal vector to the flat window and the upstream direction (see Fig. 1, right). At a 90 deg elevation angle, the flat window is flush with the upstream floor of the test section. The 2 by 4 in. flat window on the cylinder has an optically accessible portion measuring 1.5 by 2.5 in. The streamwise x coordinate

originates from the cylinder center, and the cross-stream y coordinate is vertical with zero at the floor of the test section upstream of the turret (see Fig. 1, right).

The test section was instrumented with eight static pressure ports to monitor the streamwise variation of the velocity for different elevation angles. The pressure ports were placed in the streamwise direction, 1 in. apart from each other, along the line $y = 1.875$ in.: that is, approximately halfway between the top wall and the bottom wall upstream of the turret (see Fig. 1, left).

A range of incoming Mach numbers between 0.4 and 0.7 were used to investigate the optical aberrations. To achieve these conditions, the flow in the tunnel test section was driven by up to three Allis Chalmer 3310 ft^3 / min vacuum pumps with variable valve settings between the test section and the vacuum plenum.

III.   Results

A.   Velocity Results

The cross-stream profiles of the streamwise component of the velocity or, to be exact, the velocity component normal to the hot wire, $(u^2 + v^2)^{1/2}$, were measured at several streamwise locations for three elevation angles of 90, 100, and 120 deg with a single hot wire. All hot-wire measurements were performed for an incoming Mach number of 0.4, and data were collected at each point for 10 s at 100 kHz.

The boundary layer at $x/R = -1.25$ upstream of the cylinder centerline had a displacement thickness δ^* and momentum thicknesses Θ of 0.8138 and 0.6909 mm, respectively. The maximum boundary-layer fluctuating velocity had a normalized turbulence level of 0.08.

At the 90 deg case, the turret flat window was flush with the upstream portion of the test section floor, so the boundary layer continued to develop as it moved downstream (see velocity profiles shown in Fig. 2, upper row). Normalized turbulence levels for all locations above the flat window were found to be consistent with the developing turbulent boundary layer, with a maximum value of approximately 0.08.

Results for the 100 deg elevation angle are shown in Fig. 2 (middle row). At this mild 10 deg backfacing angle, the flow formed a weak separation bubble at the window's leading edge but was reattached by the end of the flat window. The velocity profiles showed a growing boundary layer along the flat window. Normalized turbulence levels were increased downstream at this angle, ranging between 0.19 and 0.26.

Figure 2 (bottom row) shows the results for the 120 deg elevation angle. At this 30 deg backfacing angle, the flow was fully separated over the flat window and formed a large separation region downstream of the turret. Normalized turbulence levels peaked at approximately 0.18 in the shear layer, more than twice the value of the upstream boundary layer. Downstream development of the shear
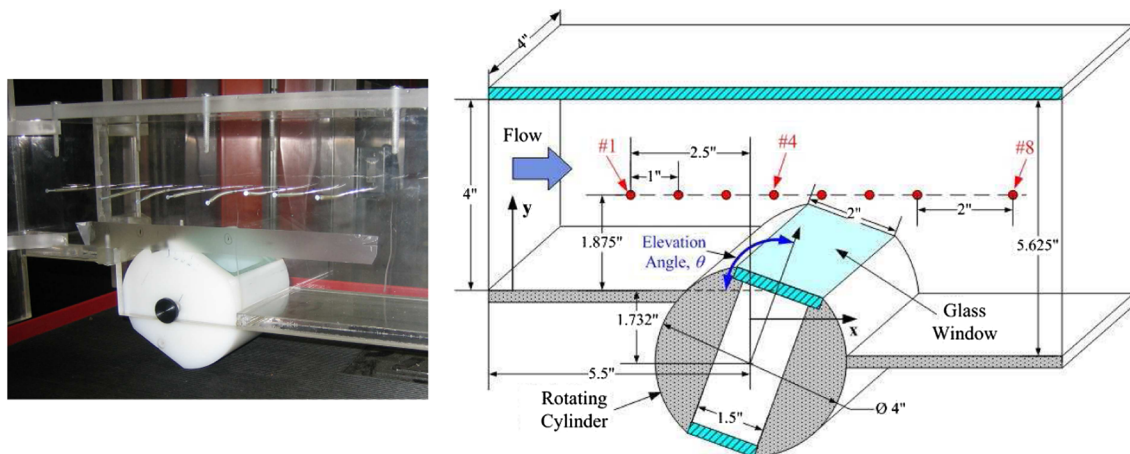

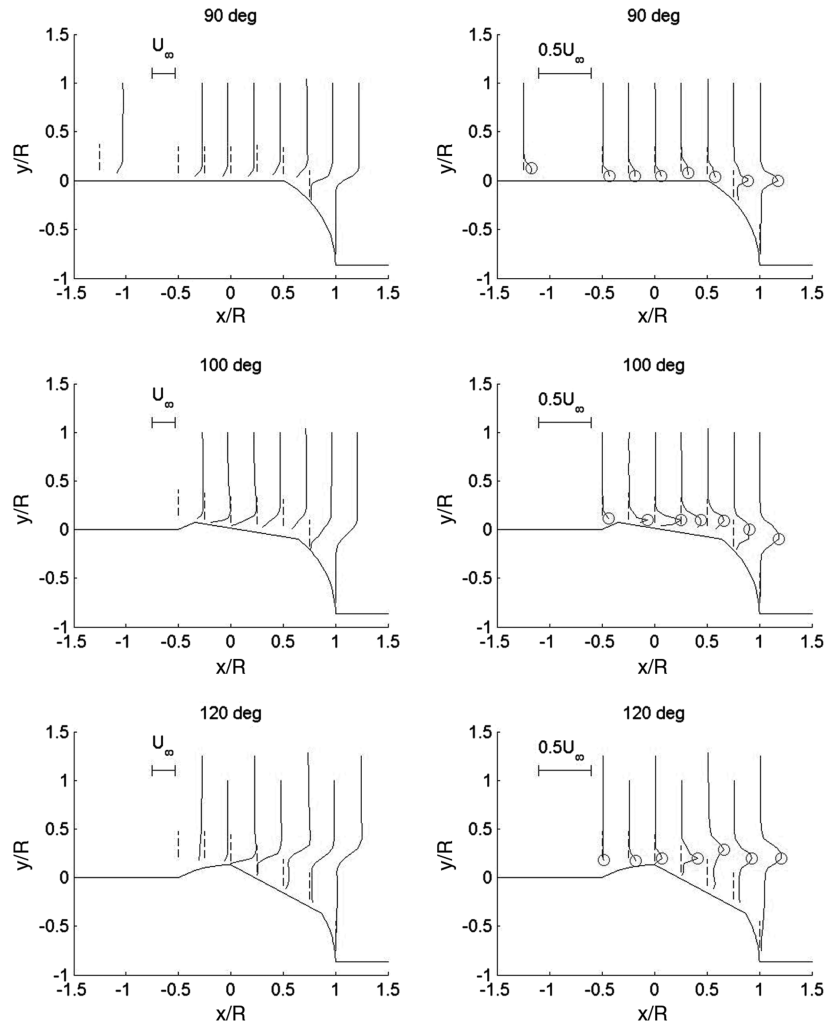**Fig. 1   Cylindrical turret, test section (left) and schematic (right).**

Fig. 2 Normalized mean velocity profiles around the cylindrical turret at different elevation angles (left column). Fluctuation velocity profiles around the cylindrical turret at different elevation angles (right column). Measurement locations are marked by dashed lines, and locations of the maximum turbulent intensities at each streamwise station are marked by circles.

layer can be clearly seen, with an almost stagnant flow near the window surface.

Mach number distributions along the sidewall of the test section, shown in Fig. 3, also clearly confirm the existence of different flow patterns around the turret for different elevation angles. In the case of the attached flow over the window (92 deg case), the flow did not change significantly in the streamwise direction, except a slight deceleration just before separating at the downstream edge of the window. In the case of the weak separation (100 deg case), the flow accelerated around the turret and over the separation bubble, but it reattached further downstream on the window. This caused the streamlines to be deflected downward, decreasing the freestream
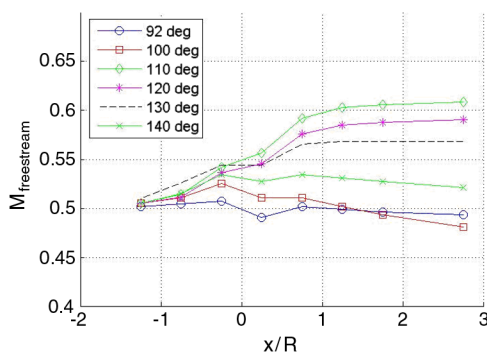

Fig. 3 Mach number distribution along the test section at different elevation angles. Incoming Mach number is 0.4.

speed downstream of the turret. In the case of the strong separation (above 110 deg), the flow separated at the leading edge of the window and remained separated downstream. For 110 and 120 deg, the initial portion of the cylinder worked as a ramp and deflected streamlines upward, causing the freestream Mach number to increase downstream. For elevation angles above 130 deg, the flow separated on the cylinder top before the front edge of the flat window, and the flat window was fully engulfed in the separated region behind the cylinder. Thus, for these high elevation angles, the flat window does not significantly affect the flow topology downstream of the cylindrical turret; therefore, the streamlines stayed parallel to the test section walls, and Mach numbers did not change downstream.

Velocity profiles for different elevation angles just downstream of the turret at $x/R = 1$ are shown in Figs. 4a and 4b. At this location, regardless of the elevation angle, all profiles are consistent with a shear layer. The location of the shear layer is approximately given by the y location of the maximum fluctuating velocity. The vertical displacement of the shear layer for different elevation angles gives an indication of the upstream flow conditions. With an angle of 90 deg, the shear layer was centered vertically with the upstream floor wall and the flat window. Increasing the elevation angle by 10 to 100 deg shifted the shear layer down by an amount equivalent to the vertical displacement of the flat-window trailing edge, indicating that the flow was attached by the end of the flat window for this mild backfacing angle. At 110 deg, the shear layer was shifted upward by approximately $y/R = 0.25$. This shift is equivalent to the vertical displacement of the leading edge of the flat window, indicating that the flow separated at or near the leading edge of the flat window. Results for the elevation angle of 120 deg are very similar to the
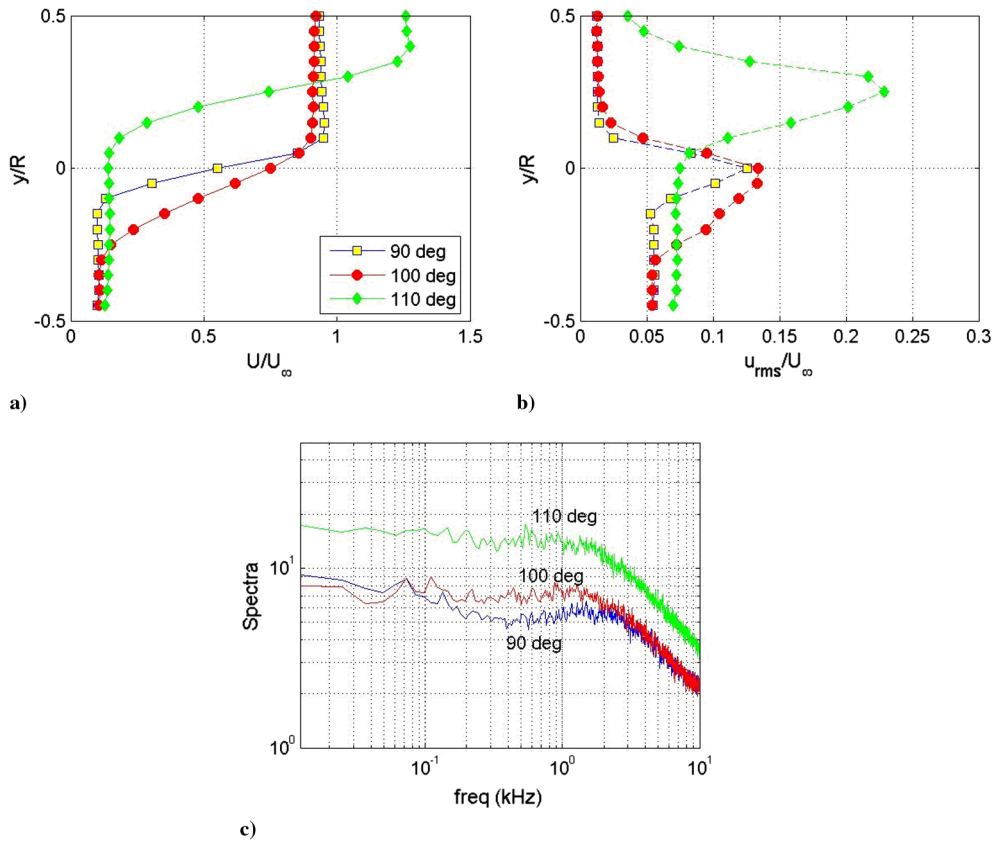
Fig. 4   Location of the maximum fluctuating velocity at $x/R = 1$ for turret elevation angles of 90, 100, and 110 deg: a) normalized mean, b) fluctuating velocity profiles, and c) velocity spectra. Incoming Mach number is 0.4.

results at 110 deg and, therefore, are not shown here. All these observations are consistent with the flow topology at different elevation angles discussed before.

Velocity spectra at the location of the maximum fluctuating velocity for 90, 100, and 110 deg are shown in Fig. 4c. At the lowest elevation angle of 90 deg, the velocity spectrum shows the presence of energetic structures up to several kilohertz, with a weak hump around 1.5 kHz. The spectral energy increases with the increasing elevation angle, and the location of the hump moves to approximately 1 kHz for the elevation angles of 100 and 110 deg. It indicates that the dominant streamwise structure in the separated shear layer at $x/R = 1$ grows in both energy and size.

The surface oil flow visualization performed downstream of the turret (not presented here) showed that, at elevation angles of 90 and

100 deg, the separation bubble reattached to the bottom of the test section at approximately $x/R = 7, \dots , 8$. The separated flow behind the turret at the elevation angle of the 120 deg case was reattached further downstream, around $x/R = 8, \dots , 9$. Velocity profiles measured at two downstream locations of $x/R = 8.25$ and 13.25 are shown in Fig. 5. For the elevation angles of 90 and 100 deg, the flow was already attached by the $x/R = 8.25$, and by $x/R = 13.25$, the velocity profiles were virtually indistinguishable. For the 120 deg case, the flow was reattached around the first location of $x/R = 8.25$, so the mean normal shear stress dU/dy was found to be approximately zero at this streamwise location. At both locations, the high-speed side of the shear layer, which was considered as the local freestream speed, was higher than the local freestream speeds for the elevation angles of 90 and 100 deg due to the blockage effect from the
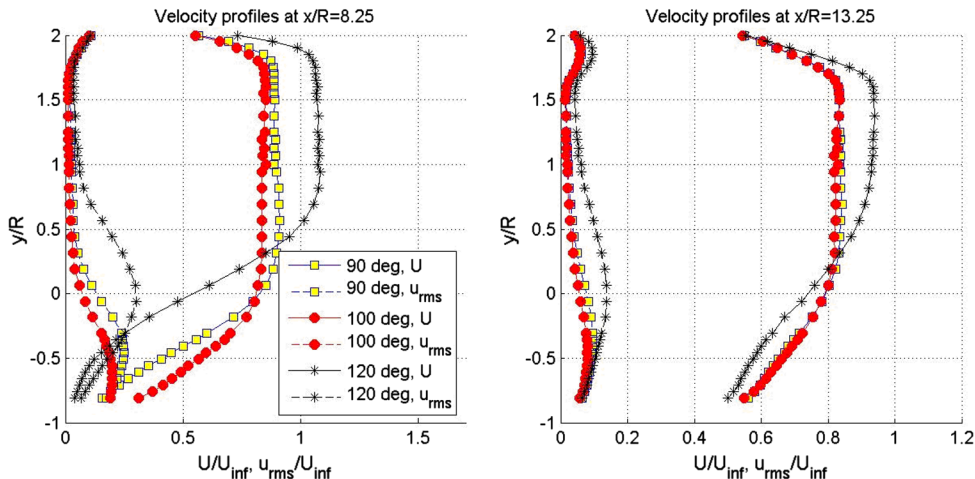

Fig. 5   Normalized mean and fluctuating component of velocity downstream of the cylindrical turret at elevation angles of 90, 100, and 120 deg.

more protruding cylinder and the resulting upward-displaced shear layer. Finally, the boundary layer at the top wall of the test section is also visible in Fig. 5, between $y/R = 1.7..2$ for all elevation angles.

B. Wavefront Measurements

To measure optical distortions through the flat window, a Wavefront Sciences CLAS-2D two-dimensional (2-D) Shack–Hartmann-type wavefront system was used. The schematic of the 2-D wavefront optical setup is presented in Fig. 6. A circular laser beam, 2 in. in diameter, was directed through the flat window and normal to it. A return mirror outside of the test section was used to coaxially return the laser beam back to the optical bench. Thus, the beam propagated through the turbulent flow twice, doubling the signal-to-noise ratio. After the returning beam was deflected out of the incoming beam train using a cube beam splitter, the beam's optical distortions were measured using the 2-D wavefront sensor, making use of 33×33 of the sensor's 33×44 lenselet array. The wavefronts were made using a pulsed frequency-doubled neodymium–doped-yttrium-aluminum-garnet laser with a pulse width of 5 ns. The wavefronts were sampled at 10 Hz. Several hundred wavefronts were recorded for each of the different elevation angles between 90 and 150 deg and the range of incoming Mach numbers between 0.4 and 0.7. Piston, tip/tilt, and mean lensing were removed from each wavefront, and the fluctuating parts of the optical wavefronts were computed. Levels of optical distortions were characterized by an ensemble-averaged spatial root-mean square of the fluctuating optical path difference (OPD):

Fig. 6   Schematic of optical setup.

$$\mathrm{OPD}_{\mathrm{rms}} = \left[\left\langle \int_{Ap} \mathrm{OPD}^2(x,y)\, dx\, dy \right\rangle \Big/ \int_{Ap} dx\, dy \right]^{1/2}$$

In [3], the dimensional analysis was used to suggest that, for subsonic flows and self-similar geometries, $\mathrm{OPD}_{\mathrm{rms}}$ should be proportional to the freestream density ρ, the square of the freestream Mach number M, and a characteristic length of the geometry L, $\mathrm{OPD}_{\mathrm{rms}} \sim \rho M^2 L$; this scaling was shown to be correct for turrets [3] and boundary layers [9]. Overall levels of tip/tilt-removed optical distortions, $\mathrm{OPD}_{\mathrm{rms}}$, at several elevation angles and Mach numbers are presented in Fig. 7 (left). It can be seen that the Mach number does not affect the OPD dependence on elevation angle but simply amplifies the optical aberrations. Thus, the ρM^2, dependence is also valid for the flow around the cylinder turret, except for high transonic Mach numbers. To explain these higher than expected levels of optical aberrations at transonic speeds, a simple inviscid calculation of the 2-D flow around the cylinder at high elevation angles was performed. The lowest value of the incompressible pressure coefficient of approximately $Cp = -0.8$ was found to be on top of the cylinder, where the flow had the fastest local speed due to the cylinder curvature and, in a lesser degree, the tunnel blockage. Performing the analysis outlined in [3], the critical incoming Mach number (that is, when the supersonic region starts appearing on top of the cylinder) for this Cp is about 0.62, and the corresponding $(\rho/\rho_{\mathrm{SL}})M_{\mathrm{turret}}^2$ is approximately 0.4. Since wavefronts were measured at a higher than the critical Mach number of $M = 0.7$, the increase in optical distortions in Fig. 7 (left) is due to a local supersonic region formed around either the leading corner of the flat window of the cylinder for low elevation angles or on top of the cylinder for high elevation angles; dramatic density changes, increased turbulence levels in shocks in the supersonic region, as well as a premature shock-induced flow separation greatly increase optical distortions [3]. A similar effect was experimentally observed at high transonic speeds around hemispherical turrets [10].

The optical aberrations as a function of the elevation angle are presented in Fig. 7 (right). $\mathrm{OPD}_{\mathrm{rms}}$ are normalized by $\frac{\rho}{\rho_{\mathrm{SL}}} M_{\mathrm{turret}}^2 D$, where ρ_{SL} is the sea level density (1.225 kg/m^3), D is the turret diameter, and M_{turret} is the freestream Mach number over the turret: that is, at $x/R = 0$. From Fig. 7 (right), it is clear that the level of optical distortions strongly depends on the elevation angle. Tilt-removed $\mathrm{OPD}_{\mathrm{rms}}$ are small for elevation angles just above 90 deg but grow fast and reach a maximum around 100 deg. For higher elevation angles, the level of optical distortions exhibits a sudden drop in amplitude, then it increases slowly with the elevation after that.

To explain this behavior, recall that the flow topology is dominated by the separation bubble over the flat window, and its size strongly depends on the elevation angle (see Fig. 8). At elevation angles near 90 deg, the flow remains attached over the flat window, thus imposing only small optical aberrations due to the boundary layer over the window [9]; however, for elevation angles larger than 90 deg, as
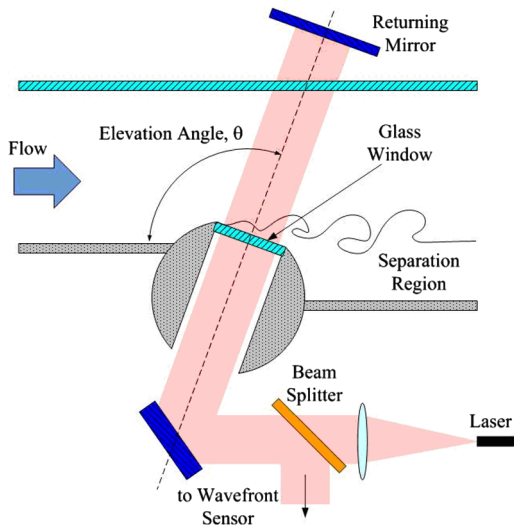

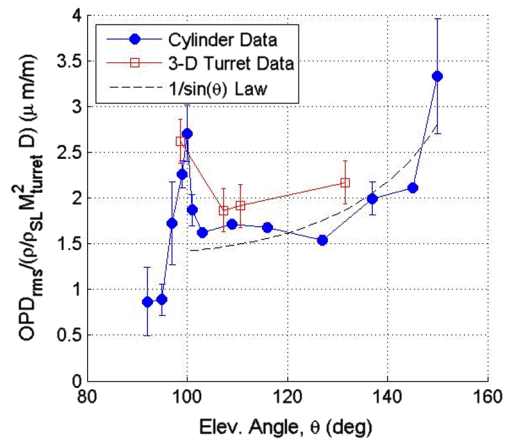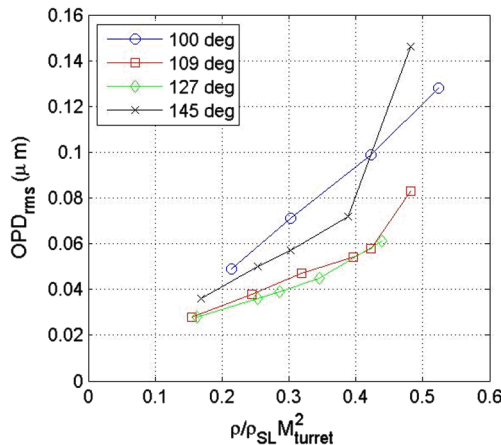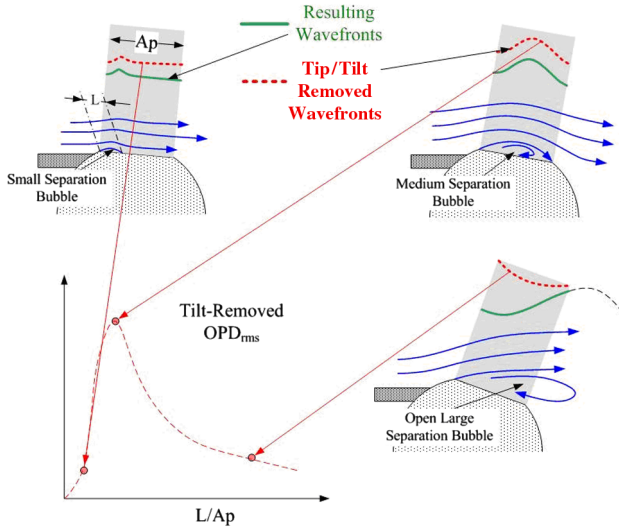**Fig. 7 $\mathrm{OPD}_{\mathrm{rms}}$ as a function of ρM^2 for selected elevation angles (left). Normalized $\mathrm{OPD}_{\mathrm{rms}}$ as a function of elevation angle (right). Normalized $\mathrm{OPD}_{\mathrm{rms}}$ from a 3-D turret with a flat window [7] is also shown for comparison.**

Fig. 8 Top: Flow topologies, overall and tip/tilt-removed wavefronts for different elevation angles.

discussed in the previous section, the flat-window aperture works as a backfacing ramp with an adverse pressure gradient that, combined with the slope discontinuity in the beginning of the flat window, creates an unsteady, closed separation bubble formed at the leading edge of the window and the reattachment point on the aperture. When the elevation angle increases, the separation bubble grows in size and strength, and the reattachment point moves downstream. At some elevation angle, the reattachment point reaches the end of the flat window, and the separation bubble becomes an open separated region extending downstream beyond the cylindrical turret, and it forms a separated shear layer that originates from the leading edge of the flat window and extends downstream.

When the separation bubble is bigger than the window length, its underlying large vortical structure, while still creating larger levels of resulting optical aberrations, exerts mainly tip/tilt distortions on the laser beam (see Fig. 8, lower right plot). As the overall tip/tilt is removed from OPD$_{rms}$, the level of residual tip/tilt-removed wavefronts drops for elevation angles above 100 deg, which is observed in Fig. 7. Therefore, the spike in OPD$_{rms}$ around 100 deg is related to aperture effects, when the structure size is larger then the laser beam size [11]. Increasing the elevation angle even further forces the laser beam to go though the separated shear layer at an increasing oblique angle and effectively increases the distance it travels through the region of the turbulent shear layer. From geometrical considerations, it follows that optical aberrations should go up as $\sim 1/\sin(\theta)$. The experimental data, shown as a solid black line in Fig. 7, verify this theoretical trend, at least for the measured elevation angles up to 140 deg. At 150 deg, however, there is a rise in

the curve that might indicate that the shear layer starts growing downstream. This is contrary to the situation at less than 140 deg, where the $1/\sin(\theta)$ law assumes that the shear layer is approximately the same thickness over the window. It should be noted in Fig. 7 that optical data from a three-dimensional (3-D) flat-window hemispherical turret, reported in [7], are also included; these will be discussed later.
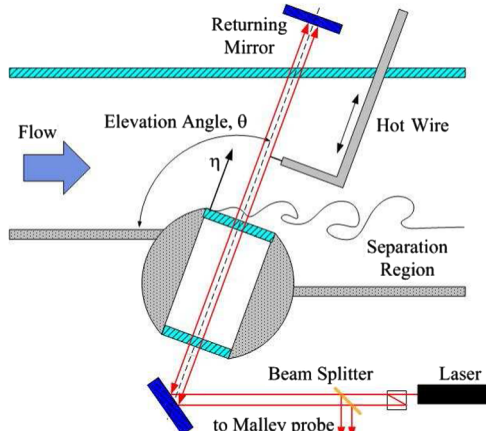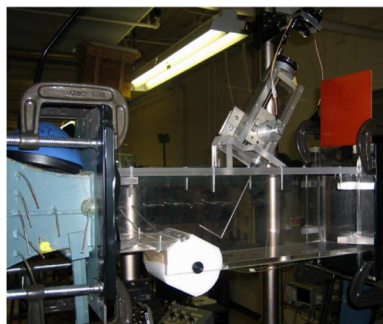
C. Malley Probe/Hot-Wire Correlation

Simultaneous single hot-wire and Malley probe [12] measurements were also made for three elevation angles of 90, 100, and 120 deg. U velocity or, to be exact, the velocity component normal to the hot wire, $(u^2 + v^2)^{1/2}$, measurements were made normal to the turret flat window, labeled the η direction (see Fig. 9). Concurrent Malley probe measurements were made spanning the path traversed by the hot-wire probe. Data at each point were taken for 10 s at 100 kHz. This high sampling rate is necessary to properly resolve the small-scale structure in the flow, since the smallest resolved structure is $\sim$sampling $-$ frequency$/U_c$. The long time record is needed to correctly measure the time delay between Malley probe beams and, consequently, the convective speed and OPD(t) (see [4] for a complete description of the Malley probe data analysis).

Malley probe measures integrated optical aberrations across the entire flow [12] and do not provide any information about where the sources of optical aberrations are along the path. Simultaneous velocity/Malley probe measurements for the hemispherical (3-D) turret for one azimuthal angle of 110 deg were performed and reported in [4]. To compare the aero-optical environment around the cylindrical and hemispherical turret, similar simultaneous optical-velocity measurements were conducted on the cylindrical turret for several elevation angles. Velocity data were collected along the line normal to the center of the flat window at elevation angles of 90, 100, and 120, with the single hot wire traversed immediately behind the second beam. A zero-time-lag cross-correlation function between the OPD signal and the velocity data was computed using

$$\text{Corr}(\eta) = \frac{\overline{U(\eta, t)\text{OPD}(t)}}{U_{rms}^{max}\text{OPD}_{rms}} \qquad (2)$$

where OPD(t) is the OPD measured with the Malley probe, and η is the distance from the window in the normal direction. Figure 10 (left) shows the correlation function for 120 deg along with normalized mean and fluctuating components of the velocity profile. For comparison purposes, Fig. 10 (right) shows the same quantities for the hemispherical turret at the 110 deg azimuthal angle from [4]. Mean velocity profiles have similar shapes in both cases; one difference is the location of the shear layer, defined as the point where the mean velocity reaches a midpoint between the low- and high-speed values at both sides of the shear layer. For the cylindrical turret, the shear layer was located at approximately $0.3R$, where R is the turret radius, while for the hemispherical turret, the shear layer

Fig. 9 Malley probe and hot-wire setup for the 120 deg elevation angle (left) and schematic of general hot-wire/Malley probe setup (right).
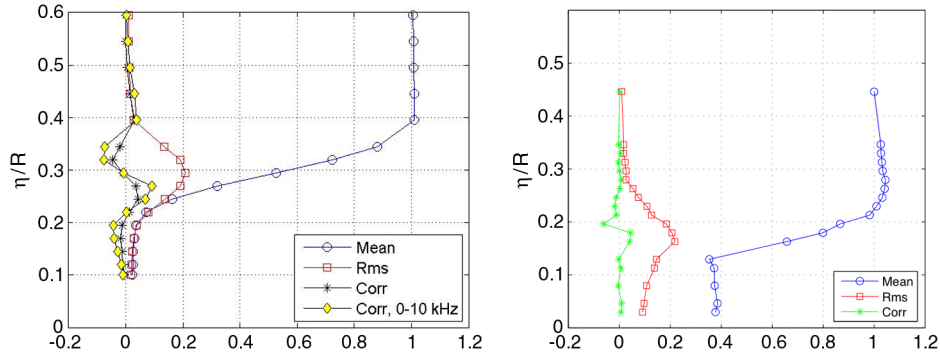
Fig. 10   Mean velocity, fluctuating velocity, and OPD–velocity correlation for cylindrical turret at 120 deg (left) and for hemispherical turret at 110 deg from [4] (right). Correlation of OPD–velocity signals, low-pass-filtered below 10 kHz, is also shown on the left.

location was $0.16R$. Another noticeable difference is a nonzero speed (about 0.4 of the freestream speed) in the recirculation zone near the window surface for the hemispherical turret case. This is due to the 3-D effects around the hemispherical turret [3], which leads to a smaller separation bubble with strong reversal flow. In both cases, the maximum velocity fluctuation is located at the middle of the shear layer, with the value of 0.2 of the freestream speed. Vortical structures at the shear layer create low-pressure wells and, consequently, lower density values inside of them [6]. Using $\text{OPL}(x) = K_{\text{GD}} \int \rho(x, s) \, ds$ from the definition of one-dimensional OPD,

$$\text{OPD}(x) = \text{OPL}(x) - \overline{\text{OPL}(x)} = K_{\text{GD}} \int \rho'(x, s) \, ds$$

It follows that $\text{OPD}(x)$ drops when the vortical structure passes over the optical path, since by the definition, $\overline{\text{OPD}(x)} = 0$ and $\text{OPD}(x) < 0$ inside the vortical structure. At the low-speed side of the shear layer, velocity fluctuations related to the passage of the vortical shear layer structure are negative, and the OPD–velocity correlation $\text{Corr}(\eta) > 0$; the shear layer velocity fluctuations are positive at the high-speed side of the shear layer with $\text{Corr}(\eta) < 0$, which is exactly the same for both the cylindrical turret (see Fig. 10, left) and the hemispherical turret (see Fig. 10, right). Low values of the OPD–velocity correlations (~ 0.06) can be explained by the fact that only low-frequency velocity components have associated pressure drops, while high frequencies do not correlate with the OPD, thus lowering the overall OPD–velocity correlation [4]. To verify that, both velocity and OPD time series were low-pass-filtered below 10 kHz, where most of the velocity spectral energy is located (see Fig. 4c), and the correlation was recalculated for the filtered signals. Results are also shown in Fig. 10 (left plot). The shape of the filtered correlation is similar to the unfiltered correlation, but the amplitude is higher, reaching levels of 0.12. Inspection of the frequency range above 10 kHz showed essentially no correlation between the velocity and OPD signals in this range and, therefore, is not shown here.

Referring back to Fig. 7, while the overall magnitude of OPD_{rms} is larger in the hemispherical turret case, the general trends are the same. Furthermore, the correlation of optical and fluctuating velocity data show very similar trends. While the flow topology around the hemisphere turret is more complicated, it is clear that the aberrating flowfields share the same physics.

IV.   Conclusions

Optical aberrations over the cylindrical turret with the flat window at backlooking elevation angles were measured using both a 2-D wavefront sensor and a Malley probe as a function of laser beam/window elevation angle. To understand the nature of the aero-optical aberrations, extensive measurements of the flow topology at different elevation angles were conducted using a single hot wire. The results show that the dominant aero-optical source is the unsteady separation bubble formed at the leading edge of the flat window. It was shown that, while the size of the bubble glows monotonically with the elevation angle, the level of tilt-removed optical distortions has a sharp peak around 100 deg, precipitously dropping after that and then

gradually increasing again at high elevation angles. As shown in [11], tip/tilt removal acts as an aperture filter, explaining the precipitous drop once the flow separates over the entire window.

This experimental study showed that qualitatively and quantitatively, aero-optical aberrations around the cylindrical turret are quite similar to the aberration around the flat-window turrets, as the underlying cause was shown to be a separation bubble over the flat window. In [7], several passive flow-control devices were tested on the cylindrical turret and the flat-window turret, and it was demonstrated that the peak in OPD_{rms} around 100 deg could be mitigated.

The cylindrical turret offers the obvious advantage of being able to more easily explore the optical flow physics shared by the hemispherical turret in both baseline and flow-control experiments, which are currently the subject of ongoing investigations, with some promising preliminary results reported in [7,13,14].

Finally, it should be pointed out that, due to geometrical simplicity and relevance to aero-optical problems, the experimental results for the flow and aero-optical aberrations around the 2-D cylindrical turret provide excellent benchmark experimental data to validate CFD studies geared toward creating reliable codes to compute aero-optical environment [15,16].

References

[1] Gilbert, K. G., and Otten L. J. (eds), *Aero-Optical Phenomena*, Vol. 80, Progress in Astronautics and Aeronautics, AIAA, New York, 1982, pp. 1–9.

[2] Duffin, D., "Feed-Forward Adaptive-Optic Correction of a Weakly-Compressible High-Subsonic Shear Layer," Ph.D. Thesis, Univ. of Notre Dame, Notre Dame, IN, 2009.

[3] Gordeyev, S., and Jumper, E., "Fluid Dynamics and Aero-Optics of Turrets," *Progress in Aerospace Sciences*, Vol. 46, No. 8, 2010, pp. 388–400.
doi:10.1016/j.paerosci.2010.06.001

[4] Gordeyev, S., Hayden, T., and Jumper, E., "Aero-Optical and Flow Measurements over a Flat-Windowed Turret," *AIAA Journal*, Vol. 45, No. 2, 2007, pp. 347–357.
doi:10.2514/1.24468

[5] Gordeyev, S., Jumper, E., Ng, T., and Cain, A., "Optical Disturbances Caused by Transonic Separated Boundary Layer Behind a 20-Degree Ramp: Physics and Control," 42nd AIAA Aeroscience Meeting and Exhibit, Reno, NV, AIAA Paper 2004-0472, 5–8 Jan. 2004.

[6] Fitzgerald, E. J., and Jumper, E. J., "The Optical Distortion Mechanism in a Nearly Incompressible Free Shear Layer," *Journal of Fluid Mechanics*, Vol. 512, 2004, pp. 153–189.
doi:10.1017/S0022112004009553

[7] Cress, J., Gordeyev, S., Jumper, E., Ng, T., and Cain, A., "Similarities and Differences in Aero-Optical Structure over Cylindrical and Hemispherical Turrets with a Flat Window," 45th Aerospace Science Meeting and Exhibit, Reno, NV, AIAA

Paper 2007-0326, 8–11 Jan. 2007.

[8] Gordeyev, S., Jumper, E., Ng, T., and Cain, A., "Aero-Optical Characteristics of Compressible, Subsonic Turbulent Boundary Layer," 34th AIAA Plasmadynamics and Lasers Conference, Orlando, FL, AIAA Paper 2003-3606, 23–26 June 2003.

[9] Cress, J., Gordeyev, S., and Jumper, E., "Aero-Optical Measurements in a Heated, Subsonic, Turbulent Boundary Layer," 48th Aerospace Science Meeting and Exhibit, Orlando, FL, AIAA Paper 2010-0434, 4–7 Jan. 2010.

[10] Vukasinovic, B., Glezer, A., Gordeyev, S., Jumper, E., and Kibens, V., "Active Control and Optical Diagnostics of the Flow over a Hemispherical Turret," 46th Aerospace Science Meeting and Exhibit, Reno, NV, AIAA Paper 2008-0598, 7–10 Jan. 2008.

[11] Siegenthaler, John P., "Guidelines for Adaptive-Optic Correction Based on Aperture Filtration," Ph.D. Thesis, Univ. of Notre Dame, Notre Dame, IN, 2008.

[12] Malley, M., Sutton, G. W., and Kincheloe, N., "Beam-Jitter Measurements for Turbulent Aero-Optical Path Differences," *Applied Optics*, Vol. 31, No. 22, 1992, pp. 4440–4443.

doi:10.1364/AO.31.004440

[13] Gordeyev, S., Jumper, E. J., Ng, T. T., and Cain, A. B., "The Optical Environment of a Cylindrical Turret with a Flat Window and the Impact of Passive Control Devices," 36th AIAA Plasmadynamics and Lasers Conference, AIAA Paper 2005-4657, June 2005.

[14] Gordeyev, S., Cress, J., Smith, A., and Jumper, E., "Improvement in Optical Environment over Turrets with Flat Window Using Passive Flow Control," 41th AIAA Plasmadynamics and Lasers Conference, Chicago, IL, AIAA Paper 2010-4492, 2010.

[15] Wang, K., Wang, M., Gordeyev, S., and Jumper, E., "Computation of Aero-Optical Distortions over a Cylindrical Turret with Passive Flow Control," 41th AIAA Plasmadynamics and Lasers Conference, Chicago, IL, AIAA Paper 2010-4498, 2010.

[16] Morgan, P. E., and Visbal, M. R., "Large Eddy Simulation Investigating Control of Flow Over a Flat-Window Cylindrical Turret," 5th Flow Control Conference, Chicago, IL, AIAA Paper 2010-4704, 2010.

M. Glauser
Associate Editor